This is a repository copy of *A 2.5D time-frequency domain model for railway induced soil-building vibration due to railway defects*.

**Article:**

# A 2.5D time-frequency domain model for railway induced soil-building vibration due to railway defects

Authors: D.P. Connolly[1], P. Galvín[2], B. Olivier[3], A. Romero[2], G. Kouroussis[3]

1. Institute for High Speed Rail and Systems Integration, University of Leeds, UK

2. Escuela Técnica Superior de Ingeniería, Universidad de Sevilla, Camino de los Descubrimientos, ES-41092 Sevilla, Spain

3. Faculty of Engineering, Department of Theoretical Mechanics, Dynamics and Vibrations, Université de Mons, Belgium

Abstract

A new hybrid time-frequency modelling methodology is proposed to simulate the generation of railway vibration caused by singular defects (e.g. joints, switches, crossings), and its propagation through the track, soil and into nearby buildings.  To create the full source-to-received model, first the force density due to wheel-rail-defect interaction is calculated using a time domain finite element vehicle-track-soil model.  Next, the frequency domain track-soil transfer function is calculated using a 2.5D boundary/finite element approach and coupled with the force densities to recover the free-field response.  Finally, the soil-structure interaction of buildings close to the line is computed using a time domain approach.  The effect of defect type, train speed and building type (4-storey office block and 8-storey apartment building) on a variety of commonly used international vibration metrics (one-third octaves, PPV, MTVV) is then investigated.  It is found that train speed doesn't correlate with building vibration and different defect types have a complex relationship with vibration levels both in the ground and buildings.  The 8-storey apartment building has a frequency response dominated by a narrow frequency range, whereas the modal contribution of the 4-storey office building is over a wider frequency band.  This results in the 8-storey building having a higher response.

Keywords: switches-crossings-joints; railway singular defects; ground-borne vibration; building vibration; 2.5D finite element railroad track; structure-borne rail vibration; rail vehicle dynamics

## 1. Literature review

Recent increases in urban railway track infrastructure construction mean that tracks are more densely populated with artefacts such as switches, crossings and rail joints (Figure 1).  This is problematic from a ground-borne vibration standpoint because the defect-wheel interface generates large forces which can propagate into nearby buildings and cause distress to occupants ([1], [2], [3], [4], [5]).  Therefore, before proposing a change to an existing track configuration, it is important to assess the potential increase in vibrations levels within nearby buildings.

To model the behaviour of wheels in contact with rail defects requires knowledge of wheel-rail interaction [6].  Typically, when investigating ground-borne vibration, linear contact models are used to predict steady-state vibration from stationary wheel-rail roughness.  This approach is

advantageous because it can be implemented in a straightforward manner in the frequency domain (e.g. using a stationary Gaussian random process [7]).

However, in the presence of singular defects, the assumption of linear contact is unrealistic and instead non-linear contact must be modelled, typically using a time domain formulation. Much of the current work in this area is highly influenced by the early works of [8], [9] and [10], and along with Hertzian contact theory, is implemented in the software suites commonly used in the rail industry (e.g. VAMPIRE, SIMPACK AND NUCARS). When simulating tangential contact, a variation of [10] is frequently used, however when considering normal contact, Hertzian theory is commonly used.

Although a large body of research is currently on-going to develop higher accuracy and more efficient wheel-rail interaction algorithms (e.g. [11], [12], [13], [14–16]), most are focused on predicting wear and rolling-contact fatigue, rather than analysing ground vibration due to singular defects. One reason for this is because wheel-rail interaction becomes more challenging to model in the case of singular defects, due to changes in the wheel and rail radii. To address this, Younesian et al. [17] proposed a model to investigate the dynamic response of bridges and vehicles during train passage. Alternatively, Zhao et al. [18] used 3D finite element modelling to investigate wheel-rail impact forces in defect zones, while Grossoni et al. [19] performed a parametric study to analyse the effect of rail joints on dynamic vehicle behaviour.

Alexandrou et al. [20] proposed a pre-processing approach to overcome the potential singularities that occur when modelling the sharp corners associated with singular defects. This was built upon by Kouroussis et al. [21], [22], who used it to analyse the effect of a variety of defect sizes and shapes on ground-borne vibration levels. Initially an entirely numerical approach was proposed, however a hybrid field procedure also followed [23]. For the entirely numerical approach, it was proposed to use a 3D time domain finite element domain to simulate free-field propagation, which can be computationally intensive.

To solve this, a variety of scoping models have been proposed to compute ground-borne vibration. One of the most common is [24], where a reference curve (vibration vs distance) is adjusted depending upon a limited number of discrete train-track-soil factors. Alternatively, Rossi and Nicolini [25] proposed a simple model to predict ground vibration, only considering Rayleigh wave contribution, while With et al. [26] proposed an entirely empirical model. Hussein et al. [27] also proposed a fast method for assessing vibrations due to underground railways, using pipe-in-pipe methods, while Verbraken et al. [28] and Triepaischajonsak et al. [29] used hybrid approaches for at-grade cases. Alternatively, Connolly et al. [30], [31] proposed a neural network based method to predict vibration at distance from rail lines by trains using a combination of synthetic data and experimental field results. Galvín et al. [32] expanded upon this neural network approach and used it to model track-ground interaction in a reduced time, by modulating the soil Green's function.

As an alternative to 3D and empirical models is the use of 2.5D modelling has become an attractive alternative ([33], [34], [35], [36], [37]). It only requires the discretisation of the track into a 2D slice, thus reducing the number of degrees of freedom compared to a fully 3D model. However, it still allows for the recovery of the 3D response through the use of a transform.

Although these methods are useful for computing ground-borne vibration levels, large computational effort is also needed to determine the propagation of ground vibration into nearby buildings [38]. This is due to the complex nature of soil-structure interaction. François et al. [39] attempted to solve this problem by using the relative stiffness between the building and soil to

circumvent the need for soil-structure interaction (SSI) modelling. Further, Hussein et al. [40] used a sub-modelling approach to avoid modelling the entire problem in a fully coupled manner. Also, Auersch [41] proposed the use of empirical transfer functions based upon the building characteristics. López-Mendoza et al. [42] built upon this and discretised the free-field vibration into the frequency range corresponding to the modes of the structure. Modal superposition was then used, thus reducing computational requirements.

This paper builds upon these previous approaches and utilises a finite element (FE) vehicle-track-soil model to determine the force characteristics of rail defects. A 2.5D model is then combined with the force density to compute the free field vibration. Finally, building response is computed considering SSI. The model is novel compared to existing studies because for the first time it provides a numerical method to quickly compute building response due to wheel-rail singularities, while considering the full source-path-receiver system. The final model is used to investigate the effect of defect type and train speed on vibration levels both in the free field and inside buildings.
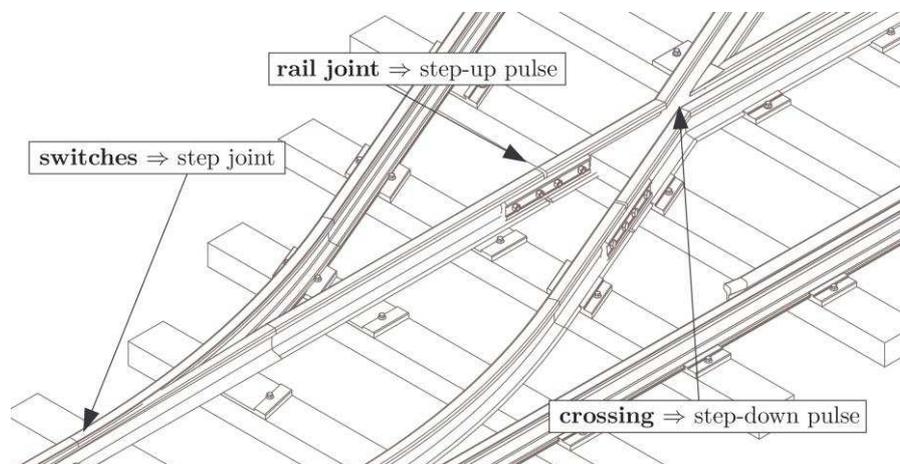


*Figure 1 – typical singular defect locations*

## 2. Numerical modelling

### 2.1. Modelling assumptions

The proposed model is developed based upon several important assumptions:

1. When a vehicle moves along a railway track, the vibrations within the track are dominated by the quasi-static response, while the vibrations in the free field are dominated by dynamic wheel-rail unevenness. For an observer at a fixed distance from the track (Figure 2 left), the resulting vibration is the sum of both the dynamic and quasi-static components generated by each individual wheel. When a train wheel impacts a localised defect (e.g. turnout or rail joint), the dynamic wheel/rail interaction force is dominant in the generation of ground vibration. This is shown in Figure 3 for a 125 km/h intercity train (AM96) passing over a rough track and a track with a localised defect (computed using a coupled multibody/finite element time domain model, aka 'MBS/FEM time domain method' [43]). It is observed that the vibration levels at 12 m from the track in terms of velocity are approximately three times higher when a localised defect is present. Similar trends are observed at other distances. Therefore this research assumes that the vibrations generated at localised defects are significantly higher than the vibrations generated due to any other source and thus all other sources can be ignored (Figure 2 right).

2. The dominance of the dynamic wheel/rail interaction at the localized defect with respect to the moving load depends on many factors, however it is strongly effected by vehicle speed. At low speed, the moving load is quasi-static and has a minor influence on the generated ground vibration [44], however at speeds above 50% of the critical velocity, this becomes more important [45]. Therefore this paper only considers cases where the train speed is low with respect to the critical velocity. This is valid because discrete rail defects are much more common on lower speed lines (e.g. tram lines) compared to high speed lines.
3. Vehicle-track-soil-building interaction can be modelling using multiple, yet coupled, sub-domains.
4. When considering the track-soil system, the track geometry is invariant in the longitudinal direction (i.e. direction of vehicle passage).
5. Force density is computed the time domain, using viscous damping for both the track and soil. Alternatively, the track-soil transfer function is computed in the frequency domain using viscous damping for the track and hysteric damping for the soil. Therefore although the track formulations are identical, they use different soil damping formulations. This is a reasonable assumption because soil damping has a low influence on the wheel-force calculation.
6. That soil-building interaction can be simulated by adding spring and damper elements to the foundations of the building model. Using this approach means stiffness and damping are independent of frequency, helping to simplify the analysis. Although some alternative approaches suggest formulations which vary with frequency, the authors have successfully shown the accuracy of this approach when studying dynamic building response in the presence of soil-building interaction. Further, reference [46] compares results from comprehensive models based on the FEM/BEM formulations and from the simplified approach used in this work. Conclusions show that structural responses are due to floor deformation, and the response if dominated by foundation area and support conditions. Alternative simplified solutions, depending on the type of foundation can be found elsewhere in the literature ([41],[47],[48],[49]). Finally, an extensive report related to this methodology can be found in [50].
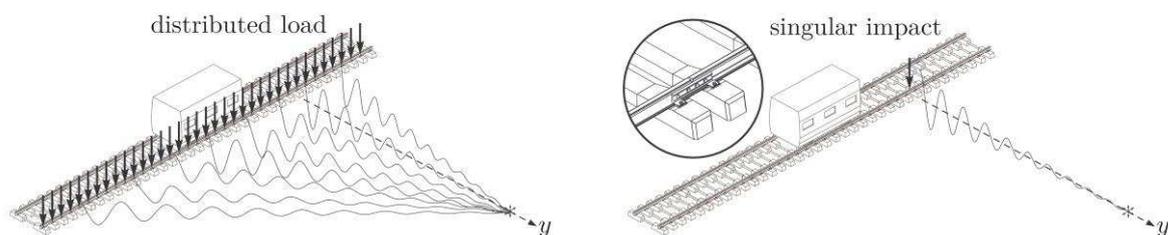


*Figure 2 – Defect excitation mechanism (Left: vibration propagation for a non-defect case, Right: vibration propagation for a defect case)*
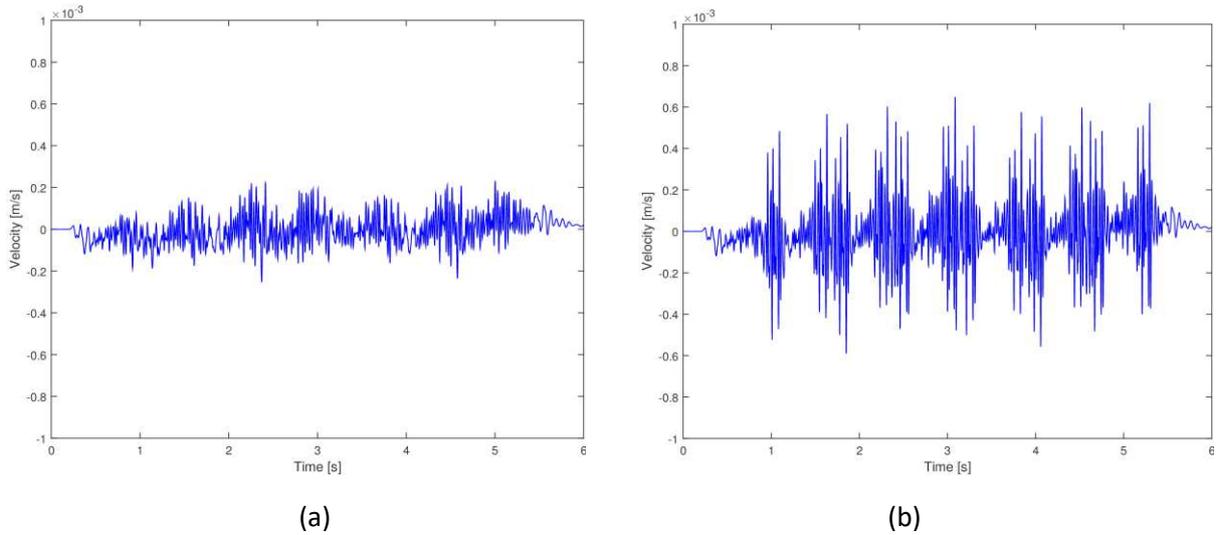
*Figure 3 – Predicted ground vibration at 12 m from the track by an AM96 train running at 125 km/h over (a) a rough track and (b) a track with a localised defect. Traces generated using model outlined in* [43]

## 2.2. Modelling approach overview

The numerical model consists of several distinct, yet coupled, systems (Figure 4). First, a MBS/FEM vehicle-track model is used to compute the force densities, $f(\omega)$, due to train passage in the presence of singular defects. Next, the track-soil transfer function, $u_{ff}(x, k_y, \omega)$ is computed, using a 2.5D boundary element (BE)/finite element modelling approach. The MBS/FEM and 2.5D models are computed independently, however the force densities and track-soil transfer function are then combined to compute the free-field soil response $u_s(x, \omega)$. Finally, the response of buildings in the free-field is computed, considering soil-structure interaction. The model is capable of generating a wide variety of internationally recognised vibration metrics, including 1/3 octave bands [51], MTVV [23][52], PPV [53], in addition to vibration time histories.
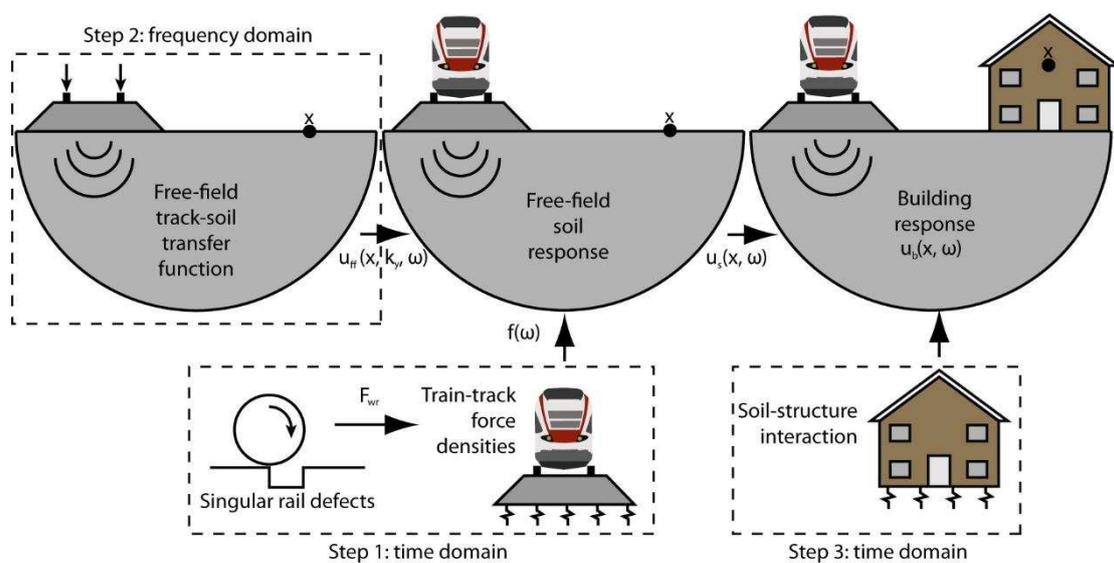


*Figure 4 – Model layout*

### 2.2.1. Step 1: train-track force densities (Vehicle-track-soil model)

*Vehicle*

The vehicle is an AM96 intercity train consisting of 3 cars as shown in Figure 5-Figure 7 and Table 1. To accurately simulate the forces generated at the singular defect it is vital that a detailed multi-body vehicle model is used [54]. Thirty degrees of freedom are considered (ten per car), using a series of springs, dampers and rigid bodies, orientated in the vertical plane (Figure 7). Such degrees of freedom are denoted $q_j$ $(j = 1, ..., n_{cp}, n_{cp})$ being the number of degrees of freedom of the vehicle (equal to 30). The equations of motion are derived using a generalized coordinates approach [55]:

$$\sum_{i=1}^{n_B} \left[ d^{i,j} \cdot (R_i - m_i a_i) + \theta^{i,j} \cdot (M_{Gi} - \Phi_{Gi}\dot{\omega}_i - \dot{\omega}_i \cdot \Phi_{Gi}\omega_i) \right] = 0, \quad j = 1, ..., n_{cp} \tag{1}$$

where, for each of the $n_B$ bodies, $m_i$ and $\Phi_{Gi}$ the corresponding mass and central inertia tensors, $R_i$ and $M_{Gi}$ are the resultant force and moment, while $a_i$ is the acceleration of the centre of gravity, and $d^{i,j}$ the partial contribution of $\dot{q}_j$ to the body velocity $v_i$:

$$v_i = \sum_{j=1}^{n_{cp}} d^{i,j} \cdot q_j \tag{2}$$

Finally, $\theta^{i,j}$ is the partial contribution of $\dot{q}_i$ to the rotational velocity $\omega_i$:

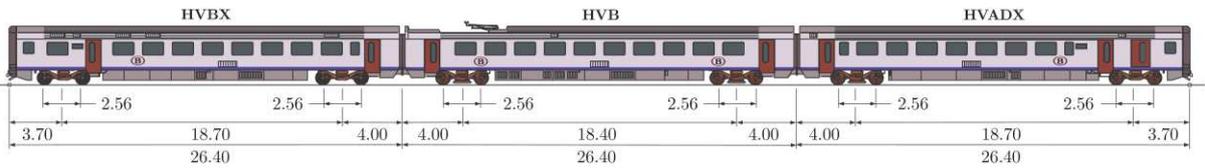$$\omega_i = \sum_{j=1}^{n_{cp}} \theta^{i,j} \cdot q_j \tag{3}$$
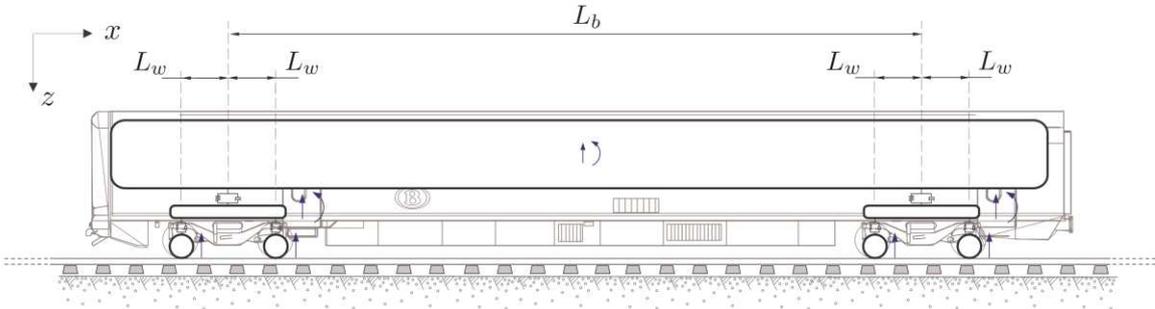


*Figure 5 – AM96 vehicle dimensions*



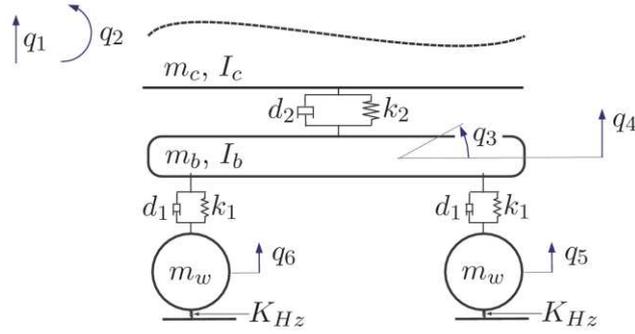*Figure 6 – AM96 vehicle assumptions*

Figure 7 – AM96 numerical bogie modelling approach

| Car | $m_c$ (kg) | $I_c$ (kg m$^2$) | $m_b$ (kg) | $I_b$ (kg m$^2$) | $m_w$ (kg) |
|---|---|---|---|---|---|
| HVB | 25,200 | 1.26x10$^6$ | 6,900 | 1.52x10$^3$ | 1,700 |
| HVADX | 28,900 | 1.45x10$^6$ | 7,050 | 1.58x10$^3$ | 1,700 |
| HVBX | 25,930 | 1.3x10$^6$ | 11,800 | 2.6x10$^3$ | 1,700 |

| Car | $k_1$ (MN/m) | $d_1$ (kNs/m) | $k_2$ (MN/m) | $d_2$ (kNs/m) |
|---|---|---|---|---|
| HVB | 1.3 | 3.7 | 0.69 | 22.6 |
| HVADX | 1.3 | 3.7 | 0.69 | 22.6 |
| HVBX | 1.81 | 1.14 | 0.69 | 14 |

Table 1 – Vehicle properties

*Wheel-rail interaction*

Singular defects cause a change in wheel and rail radii, which makes them challenging to model using traditional Hertzian theory (i.e. $R_{rail} \approx 0$, $R_{wheel} \approx 0$ at corners, and $R_{wheel} \approx \infty$ for a spot). Therefore a pre-processing step is used to solve the three-dimensional contact problem [20], before considering the contact stiffness ($K_{Hz}$):

$$K_{Hz} = \frac{nE}{3(1 - v^2)} \sqrt{\frac{8}{1/R_{wheel} + 1/R_{rail}}} \tag{4}$$

where $E$ and $v$ are the Young's modulus and Poisson's ratio of both wheel and rail materials respectively. $R_{rail}$ and $R_{wheel}$ are the radii of the rail and wheel respectively. The dimensionless parameter $n$ depends on the contact geometry (see [6] for tabular values). Four types of singular defect are considered: a step-up joint, a step-down joint, a step-up pulse and a step-down pulse. These represent the individual singular defects that comprise track artefacts such as switches, crossings, joints and changes in rail height. The profiles are shown in Figure 8, where $v_0$ is the train speed, $h$ the defect height and $l$ the defect length.
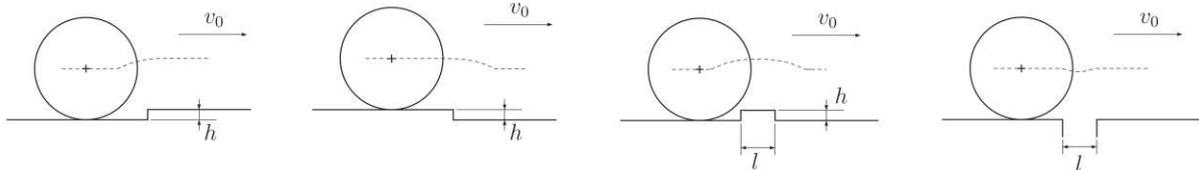


Figure 8 – Singular defect geometry (from left to right: step up, step down, positive pulse, negative pulse)

*Track/foundation*

The track is a ballasted track, however alternative track types are easily adapted. For the purposes of computing the force density, the track is modelled in two dimensions, using a Euler-Bernoulli beam for the rail. The railpad, sleepers and ballast are modelled using a series of lumped masses, springs and dampers (Figure 9). The track material properties are shown in Table 2. The presence of an embankment [56],[57] is ignored because singular defects are more commonly found at-grade in urban areas.

| Ballast track properties (2 rails) | | |
|---|---|---|
| Track gauge | 1.435 | m |
| Rail 2nd moment of area | $3.09 \times 10^5$ | $m^4$ |
| Rail Young's modulus | $2.1 \times 10^{11}$ | $N/m^2$ |
| Rail density | 7,850 | $kg/m^3$ |
| Sleeper spacing | 0.65 | m |
| Railpad stiffness per unit length (2 rails) | $6.15 \times 10^8$ | $N/m^2$ |
| Railpad damping per unit length (2 rails) | $1.2 \times 10^4$ | $Ns/m^2$ |
| Sleeper mass per unit length | 461.5 | kg/m |
| Ballast stiffness | $1.3 \times 10^8$ | $N/m^2$ |
| Ballast damping | $1.3 \times 10^5$ | $Ns/m^2$ |
| Ballast density | 1,700 | $kg/m^3$ |
| Ballast height (below sleeper) | 0.3 | m |
| Ballast cross-sectional area | 0.59 | $m^2$ |
| Ballast Poisson's ratio | 0.3 | |

*Table 2 – Ballasted track properties*

The soil supporting the flexible track model is modelled using a coupled lumped mass (CLM) model, in the vertical plane [58]. Frequency independent, analytical expressions are used to replicate the behaviour of a half-space. Five parameters (mass $m_f$, stiffness values $k_f$ and $k_c$, damping coefficients $d_f$ and $d_c$) define the CLM model and are obtained by fitting the corresponding soil response with respect to the dynamic soil parameters. Therefore, although the 5 parameters are frequency independent, the foundation behaviour has frequency dependency.
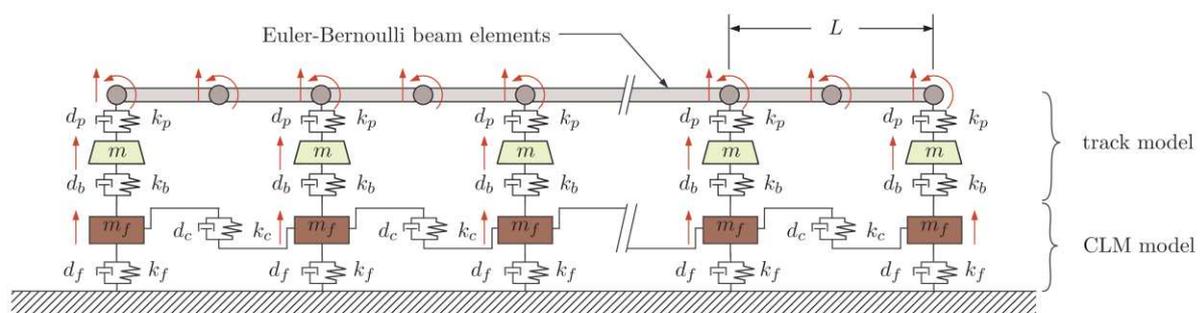


*Figure 9 – Track and soil coupling*

A discretization of $N_n$ elements per sleeper bay is used, resulting in the number of track/foundation configuration parameters $n_t$, being $(2N + 2)$ for the rail and $(2N/N_n + 2)$ for the subgrade. The following equations of motion are integrated with those of vehicle dynamics:

$$M_t \ddot{q}_t + C_t \dot{q}_t + K_t q_t = f_t$$

(5)

where $M_t$, $K_t$ and $C_t$ are the mass, stiffness and damping matrices, respectively, while $q_t$ is the configuration parameter related to track/foundation subsystem. $f_t$ represents the forces acting on the track, including the wheel/rail contact forces. The latter is therefore more accurate when taking into account the track/foundation flexibility [10].

### 2.2.2. Step 2: Track soil transfer function (Track-soil model)

A 2.5D FE-BE model is used to predict the track and free field vibrations [33] as shown in Figure 10. A domain decomposition method is used to solve the problem, where the subdomain $\Omega_b$ represents the track and the subdomain $\Omega_s$ represents the soil. The soil is modelled as a horizontally layered half-space or a homogeneous half-space. FE and BE are coupled by imposing equilibrium of forces and compatibility of displacements at the interface $\Omega_{bs}$ between both subdomains. The equilibrium equation for the dynamic soil-track interaction problem is formulated in a variational form [33]. Accounting for the equilibrium of stresses on the interface $\Omega_{bs}$ and using a finite element formulation for the interpolation of the displacement field, the governing equation is:

$$\begin{aligned}[-\omega^2 M_{bb} + i\omega C_{bb} + K_{bb}^0 - ik_y K_{bb}^1 - k_y^2 K_{bb}^2 + ik_y^3 K_{bb}^3 + k_y^4 K_{bb}^4 \\ + K_{bb}^s(k_y, \omega)]\tilde{u}_b(k_y, \omega) = \tilde{f}_b(k_y, \omega)\end{aligned}$$

(6)

Where, $K_{bb}^0$, $K_{bb}^1$, $K_{bb}^2$, $K_{bb}^3$ and $K_{bb}^4$ are the stiffness matrices, $C_{bb}$ is the damping matrix, $M_{bb}$ is the mass matrix, $\tilde{f}_b(k_y, \omega)$ is the external load vector, $\tilde{u}_b(k_y, \omega)$ is the displacement vector of the track and $K_{bb}^s(k_y, \omega)$ is the dynamic soil stiffness matrix. A tilde above a variable denotes its representation in the frequency-wavenumber domain. The dynamic soil stiffness matrix is computed using the 2.5D boundary element method.

Once the equilibrium equation for the dynamic track-structure interaction problem is solved, integral representation theory is applied to compute the radiated wave-field from the tractions, $\tilde{t}_s(k_y, \omega)$ and displacements, $\tilde{u}_s(k_y, \omega)$ at the soil-structure interface:

$$\tilde{u}_r(x, k_y, z, \omega) = \tilde{U}_r(x, k_y, z, \omega)\tilde{t}_s(k_y, \omega) - \tilde{T}_r(x, k_y, z, \omega)\tilde{u}_s(k_y, \omega)$$

(7)

where, $\tilde{U}_r(x, k_y, z, \omega)$ and, $\tilde{T}_r(x, k_y, z, \omega)$ are related to the boundary element discretization and the vector $\tilde{u}_r(x, k_y, z, \omega)$ collects the displacement components at $n_r$ receiver locations.

In the present study, the rails are represented using Euler-Bernoulli beams with a bending stiffness $E_r I_r$ and a mass $\rho_R A_r$ per unit length. Their displacements are denoted $u_{r1}$ and $u_{r2}$. The positions of the rail are determined by $y_1$ and $y_2$, with, $y_2 - y_1$, equal to the track gauge $r_d$. The internal energy dissipation in the rail is modelled using a loss factor $\eta_r = 0.05$. The rail pads are modelled as continuous spring-damper connections with a spacing of $L$. The rail pad stiffness $k_p$ of a single rail pad is used to calculate an equivalent stiffness $\overline{k_p} = k_p/L$. An equivalent damping coefficient $\overline{d_p}$ is used to account for internal energy dissipation in the rail pad.

The ballast is represented using a set of distributed linear springs and dampers. The smeared ballast stiffness $\overline{k_b}$ is computed from the vertical spring stiffness $k_b$ per sleeper as $k_b/L$. An equivalent damping coefficient is computed as $\overline{d_b} = d_b/L$. The equivalent ballast mass $m_b$ is computed from the ballast mass $m_b$ situated under each sleeper as $m_b/L$. The concrete sleepers are assumed to be rigid in the plane of the track cross section, so that the vertical sleeper displacements along the track are determined by the vertical displacement $u_{sl}$ and rotation $\beta_{sl}$ at the centre of gravity of the sleeper. The sleepers are modelled as a uniformly distributed mass $\overline{m} = m/L$.

For the slab track case, the slab is represented by an Euler-Bernoulli beam with a bending stiffness $E_{slab}I_{slab}$ and a mass $\rho_{slab}A_{slab}$ per unit length.

The soil is modelled as an elastic half-space. At the interface between the embankment and the soil, relaxed boundary conditions are assumed, so that only continuity of the vertical displacements is imposed.
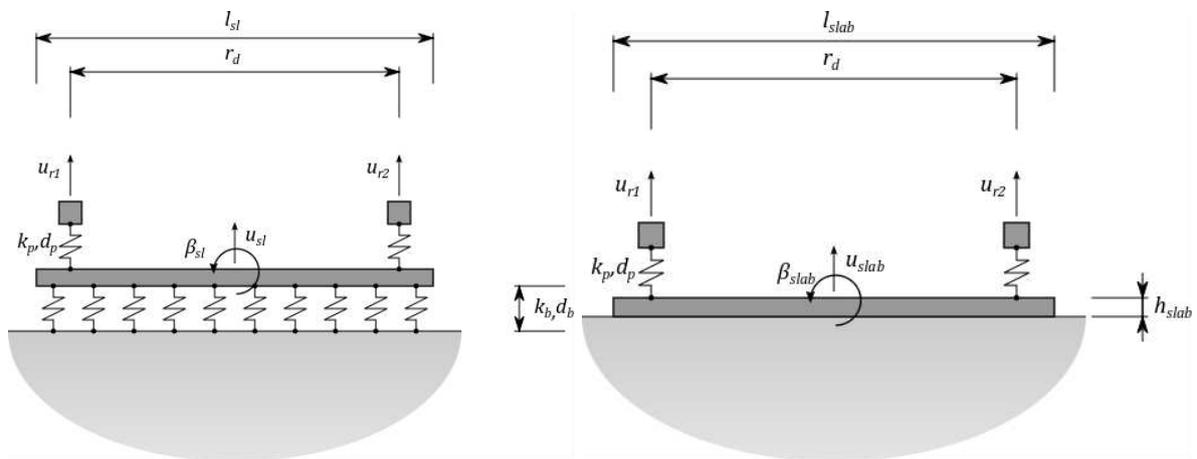


*Figure 10 – 2.5D track-soil models (left: ballast, right: slab)*

### 2.2.3. Step 3: Soil-structure interaction (Soil-building model)

The soil-structure interaction of buildings nearby the railway line is computed using the soil response, calculated using the previous steps. The structural response is obtained by the SSIFiBo toolbox [59] based on a 3D time domain FEM methodology. To do so, the frequency domain soil response is transformed to the time domain using an inverse FFT. The soil response is computed from 0Hz to 500Hz using a frequency step of 0.25Hz. Therefore the time domain response is computed from 0s to 4s, using a time-step of 0.001s (sampling frequency=1000Hz). This time-step allows for the building response to be computed with high accuracy. Alternatively, it can be computed without any inverse transformation using the methodology proposed in [42].

A 4-storey office building and an 8-storey apartment building are considered, each with a footprint of 12mx12m (Figure 11). Each storey is 3m tall resulting in building heights of 12m and 24m, for the 4 and 8 storey buildings respectively. Both buildings are comprised of concrete columns (0.6mx0.4m), four edge beams (0.6mx0.2m) and two framed concrete walls (2.4mx0.15m). The floors are simply supported slabs, of thickness 0.2m, axial stiffness per unit length $1.433 \times 10^9$ N/m, bending stiffness per unit length $9.935 \times 10^6$ Nm and a mass per unit area of 172kg/m². Two-node Euler-Bernoulli elements are used to model the beams and columns, while four-node shell elements are used for the floors and walls. Soil-structure interaction is considered using spring and damper elements by a simplified methodology [50]. The stiffness $K_f$ and damping $D_f$ of the foundation are [41]:

$$K_f = 3.4 G_s \sqrt{A_f}$$

$$D_f = 1.6 \sqrt{G_s \rho_S A_f}$$

where $A_f$ is the foundation area, and $G_s$ and $\rho_S$ are the soil shear modulus and mass density respectively. The dominant mode shapes are shown in Figure 12 and Figure 13, while the corresponding participation factors are shown in Table 3 and Table 4. It is seen that the 8 storey building response is governed by lower frequencies than the 4 storey building.
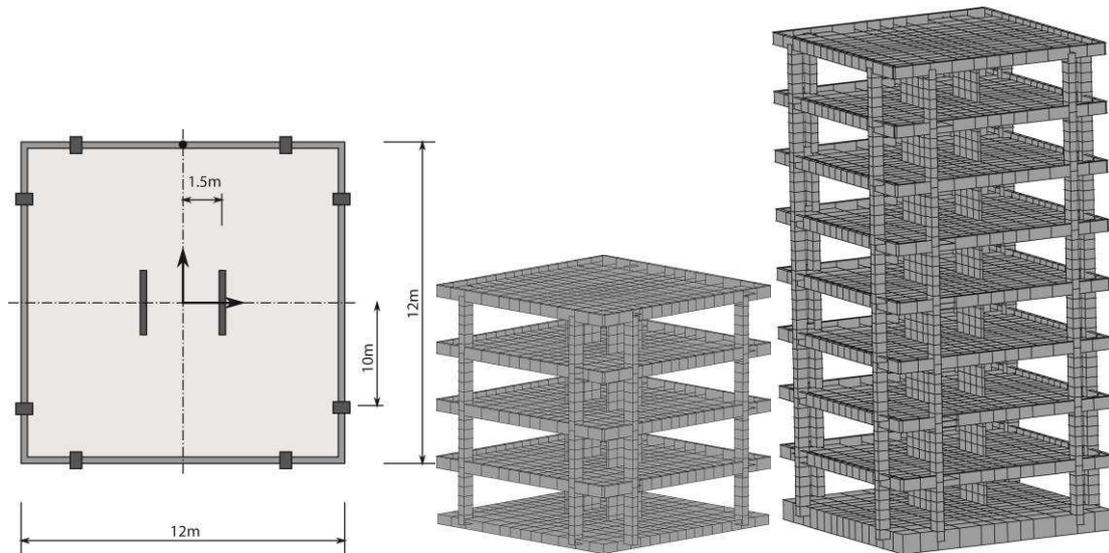


*Figure 11 – Four and eight storey building layouts (Left: building foundation, Middle: 4 storey, Right: 8-storey)*

| 4 storey | | |
|---|---|---|
| Mode # | Frequency (Hz) | Participation factor (%) |
| 6 | 11.94 | 3.93 |
| 10 | 13.26 | 4.18 |
| 14 | 13.93 | 12.53 |
| 17 | 14.25 | 18.04 |
| 33 | 28.82 | 35.02 |
| 44 | 33.46 | 3.57 |
| 51 | 36.39 | 2.98 |
| 74 | 50.63 | 8.97 |
| 80 | 60.38 | 7.81 |

*Table 3 – 4-storey building participation factors*

| 8 storey | | |
|---|---|---|
| Mode # | Frequency (Hz) | Participation factor (%) |
| 12 | 11.46 | 39.68 |
| 17 | 12.35 | 19.74 |
| 34 | 14.41 | 3.4 |
| 52 | 20.67 | 16.69 |

| 73 | 30.19 | 7.49 |
|---|---|---|

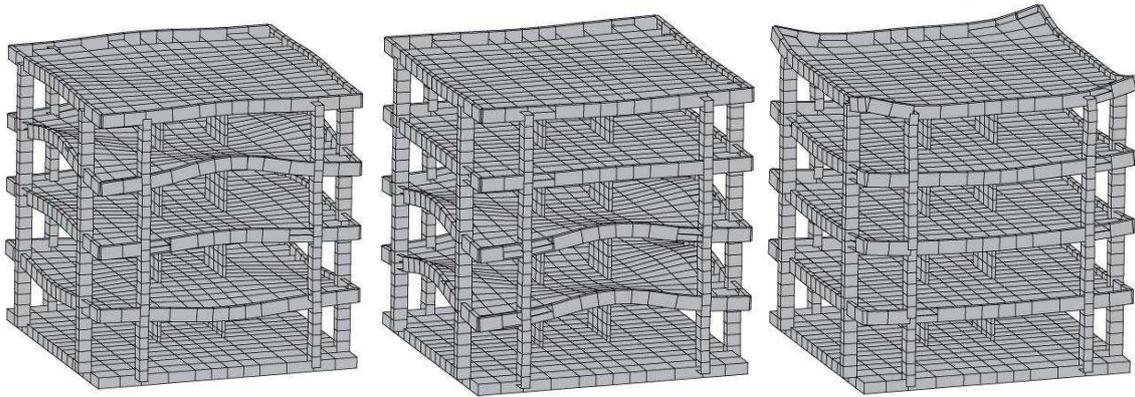Table 4 – 8-storey building participation factors



Figure 12 – Dominant 4-storey building mode shapes (left: mode 14, middle: mode 17, right: mode 33)
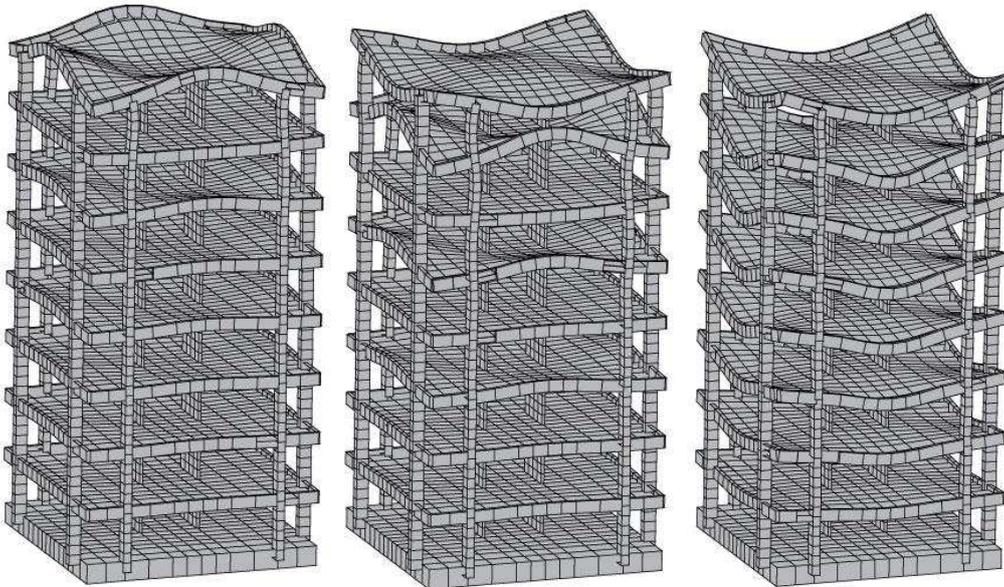


Figure 13 - Dominant 8-storey building mode shapes (left: mode 12, middle: mode 17, right: mode 52)

## 3. Model Validation

To validate the proposed approach, the case described in the "modelling assumption" section is used. Track and soil parameters are given in [29]. Figure 3(b) presents the ground vibration computed using a MBS/FEM time domain model [29] while Figure 14 shows the results from the proposed hybrid time-frequency method. A similar shape is obtained, with maximum amplitude agreement, validating also the hypothesis of wheel/rail interaction force at localized defects as the main contributor to ground vibration.

*Figure 14 – Model validation: velocity time history at 12 m from the track generated by an AM96 train running at 125 km/h a track with a localised defect*



*Figure 15 – Field measurement of track receptance [43]*
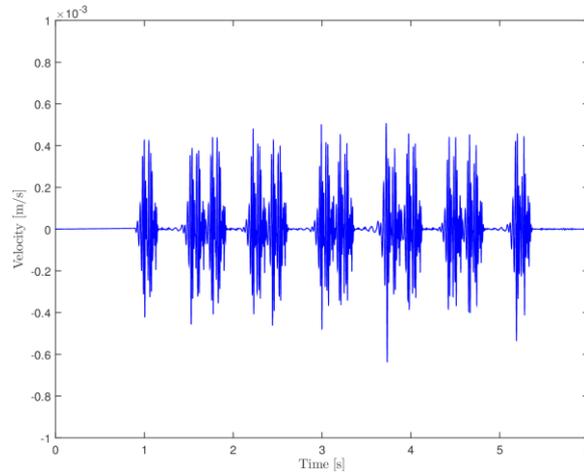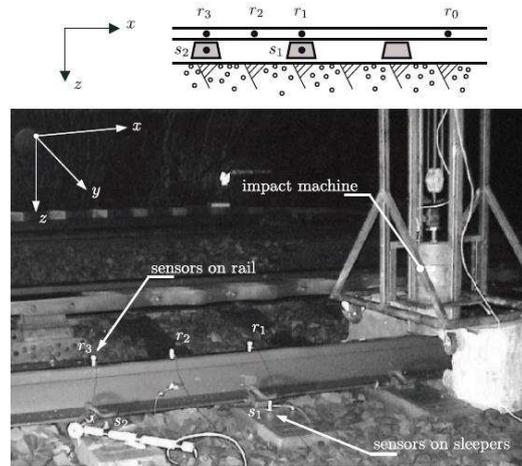
Figure 15 presents PPV (Figure 15 left) and RMS level (Figure 15 right) as a function of the distance from the track. The black line shows the data collected during an experimental campaign performed on the L161 line in Brussels, Belgium. An example of the track receptance test procedure is shown in Figure 15, while the test procedure and results are described comprehensively in [43]. Figure 15 shows that the correlation between the proposed hybrid model and the field measurement is acceptable, particularly considering the RMS result. Further details of model validation can be found in [60].

In addition, two additional datasets are plotted on the same figure using the MBS/FEM time domain method. These consider:

1. The passing of the AM96 vehicle over a rough rail without a singular defect. This result is named, 'static contribution', because it includes the quasi-static excitation and the dynamic excitation due to unevenness, but not the excitation due to the singular defect
2. The passing of the AM96 vehicle over a rough rail with a singular defect. This is named, 'all contributions', because it includes the quasi-static excitation, the dynamic excitation due to unevenness and the excitation due to a singular defect

Point 2 is relevant because it uses the same assumption that underpins the proposed hybrid model (i.e. singular defect ground vibration can be simulated without the quasi-static contribution due to the moving load). From this, the static contribution shows, (in a similar manner as Figure 3) that the moving load effect is negligible compared to the dynamic effect generated by a wheel the passing over a localized defect.
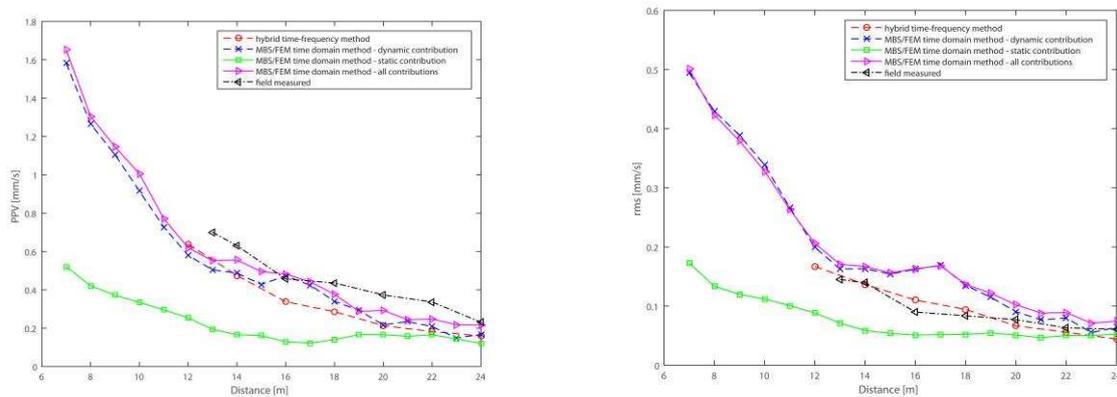


*Figure 16 – Numerical and field measured PPV (left) and RMS (right) level versus distance from track*

## 4. Analysis

Two sets of analysis are performed. The first is into the effect of defect type and train speed on ground-borne vibration. The second is into the effect of defect type, train speed and building type on building vibration. The soil is a homogenous half-space with material properties: $E = 100$ MPa, $\xi=0.05$, $v=0.35$, $\rho = 2000$ kg/m$^3$. Track parameters are given in Table 2.

### 4.1. Ground-borne vibration

### 4.1.1. Defect type effect on soil response

Four defect types are modelled as described earlier, and subject to the passage of an AM96 train at 120km/h. Figure 17 shows the vertical soil surface response at 20m from the track in terms of velocity time history, 1/3 velocity dB octaves and Running RMS weighted acceleration. In the time history figure, the individual wheel passages are clearly visible for all defect types. The 1/3 octaves show that at low frequency, both positive step joints yield greatest vibration, but at higher frequency this is less clear. Instead, at frequencies corresponding to the dynamic soil contribution (≈30Hz) the order of highest to lowest vibration levels is: positive pulse, step-down, step-up, negative pulse. In terms of Running RMS weighted acceleration at 20m distance, the positive pulse generates the highest MTVV metric, while the negative pulse generates the lowest vibration. This is true for all distances as is seen in the relationship of MTVV with distance (Figure 18), however becomes less pronounced with distance.
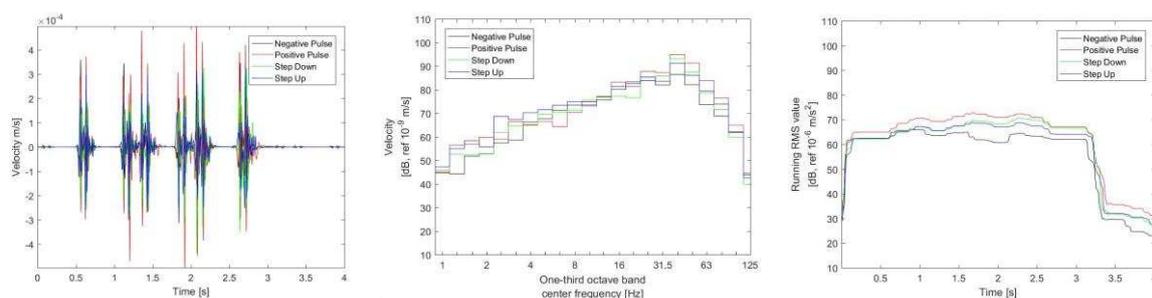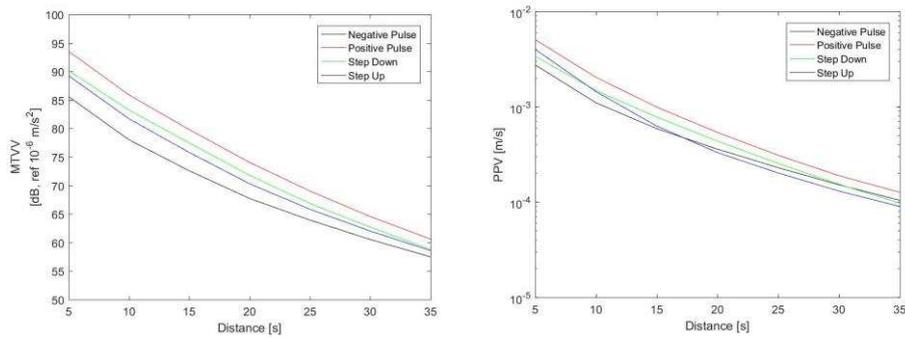
*Figure 18 - Effect of defect type on ground response with distance (Left: MTVV, Right: PPV)*

### 4.1.2.  Train speed effect on soil response

Figure 19 and Figure 20 show the effect of train speed on the vibration response caused by a negative pulse defect.  The train speeds are chosen to be significantly lower than the critical velocity of the soil to prevent low frequency amplification [45],[61][62]. One-third octaves, MTVV and PPV are again shown.  Figure 19 shows that in terms of time history, the lowest speed generates the highest peak response, and this is true for all distances as is shown in terms of PPV (Figure 20).  This speed and ground vibration independency correlates with field results collected in [63] and [64]. This is because the vehicle eigenmodes that contribute to the vehicle/track interaction forces when passing over a singular defect are dominant.

In terms of 1/3 octaves though, the lowest speed (60km/h) gives the highest response at frequencies close to 30Hz, and the lowest response at low frequencies.  Instead, the highest speed (150km/h) dominates the response at low frequency.  Further, there is a significant 1/3 octave magnitude difference between speeds at low frequency – much greater than for the different defect types previously analysed.  In terms of MTVV, the low speed train passage also generates the largest response, but its dominance diminishes with distance from the track.
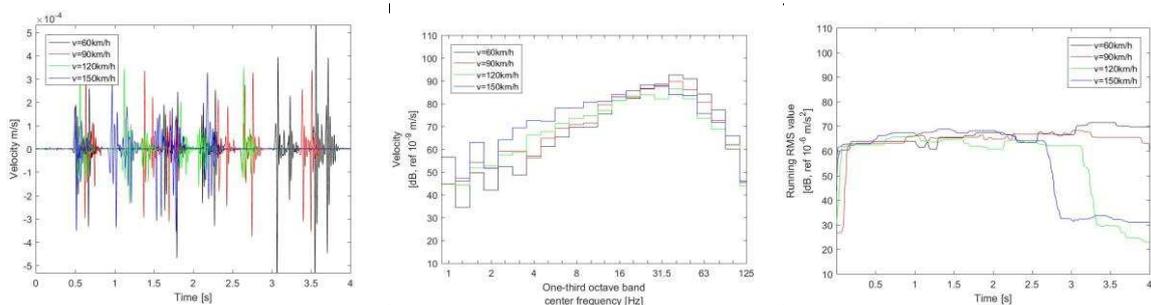


*Figure 19 – Effect of train speed on ground response (Left: velocity time history, Middle 1/3 octaves, Right: MTVV)*
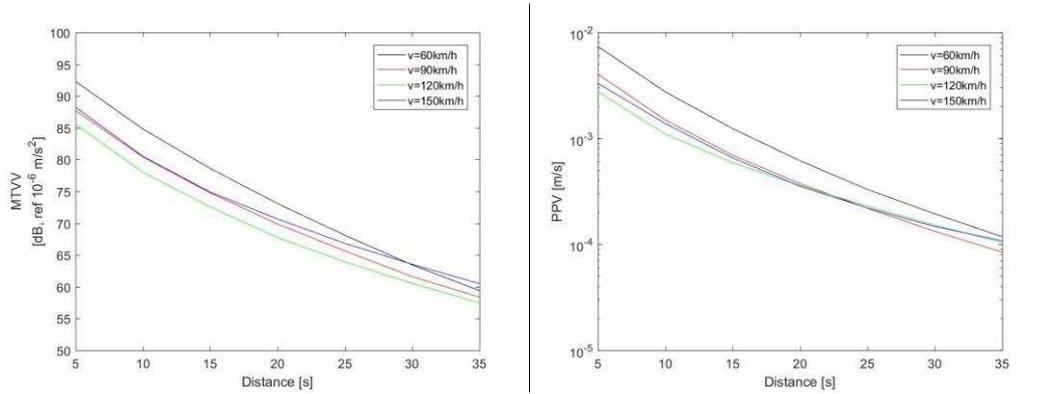
*Figure 20 – Effect of train speed on ground response with distance (Left: MTVV, Right: PPV)*

## 4.2. Structure-borne vibration

### 4.2.1. Defect type effect on building response

Figure 21 shows the effect of defect type on the vertical structural response on the top floor, (where the maximum value is expected) of the 8 storey building, at 20m from the track.  It is clear from the 1/3 octave values that the maximum vibration response is higher than that found in the ground, and at a different frequency.  The dynamic soil response at frequencies close to 30Hz is similar in magnitude, however is no longer dominant.  Instead, frequencies at 11.46Hz now dominate the response and are due to the dominant natural frequency of the building (see Figure 13 and Table 4: participation factor=39.7% at 11.46Hz), which is shown in Figure 22.  The response at 11.46Hz is ≈100dB, which is approximately 10dB greater than the maximum soil response, and 24dB greater than the soil response at 11.46Hz, in absence of the building.
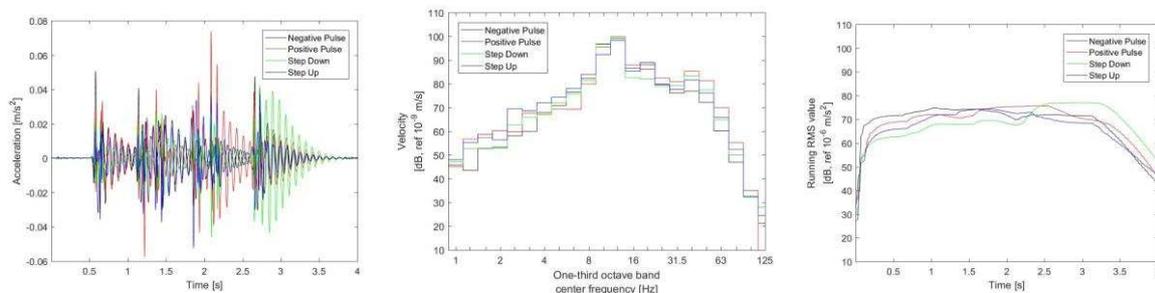


*Figure 21 – Defect type effect on building response (Left: acceleration time history, Middle 1/3 octaves, Right: MTVV)*
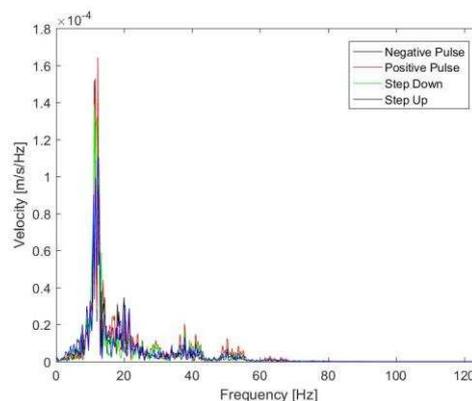


*Figure 22 – Effect of defect type on frequency content of building response*

### 4.2.2. Train speed effect on building response

Figure 23 shows the effect of four train speeds on the 8 storey building structural response. Again, the 1/3 octave values illustrate that the maximum vibration response is higher than that found in the ground, and is found at a different frequency. Frequencies close to 8Hz are now dominant due to the natural frequency of the building (Figure 24). The response at 11.46Hz is now higher than 100dB, with the highest train speed (150km/h) generating the largest vibration levels. This contrasts the previous findings regarding the soil vibration, for which the lowest speed (60km/h) produces the highest vibration levels. In a similar manner to the soil vibration case though, the low frequency vibration is dominated by the fastest speed train passage. Also, higher speeds result in elevated MTVV values. Regarding time history acceleration response, the building behaviour is more complex than for the soil and superposition is more dominant.
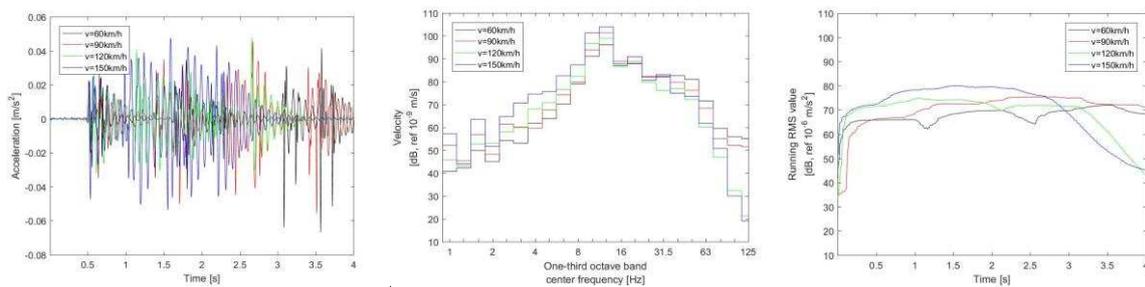


*Figure 23 – Train speed effect on building response (Left: acceleration time history, Middle 1/3 octaves, Right: MTVV)*
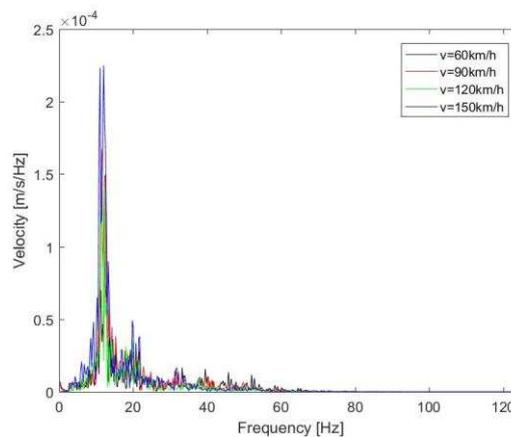


*Figure 24 – Effect of train speed on frequency response of building response*

### 4.2.3. Building type effect

Figure 25-Figure 26 show the effect of a 120km/h train passing over a negative pulse defect, on the response of 4 and 8 storey buildings. Figure 25 compares the frequency content at the top floor of each building. The 8 storey building response is over a much narrower frequency range compared to the 4 storey one, and the dominant peak is much larger. This is because the 8-storey building response is dominated by its bending floor mode shape, while the 4-storey building response is the combination of a much wider range of individual mode shapes. This agrees with the participation factor analysis because the 8-storey participation factors between 11.46-12.35Hz have 59.42% of the

energy, while for the 4-storey the participation factors between the wider frequency range of 13.93-28.82Hz have 65.59% of the energy (Table 3 and Table 4).  However, it should be noted that upon investigation of the dominant mode shapes for the 8-storey building, they are governed by the bending mode shape of the top floor (Figure 12 and Figure 13).  This is because the measurement location is within the top floor.  Therefore the dominant modes may change if a different measurement location was chosen.

Regarding one-third octaves (Figure 26 left), again it is seen that that the 8-storey building has a larger magnitude peak than the 4-storey building, and that the frequency content declines faster at high frequencies.  For the soil, there is no obvious peak at the first dominant building frequency (11-14Hz range for both buildings) and instead the peak occurs at 28.82Hz.  Figure 26 right shows the corresponding running RMS, where it is seen that the 8-storey building consistently has the highest response, while the free-field soil consistently has the lowest response.
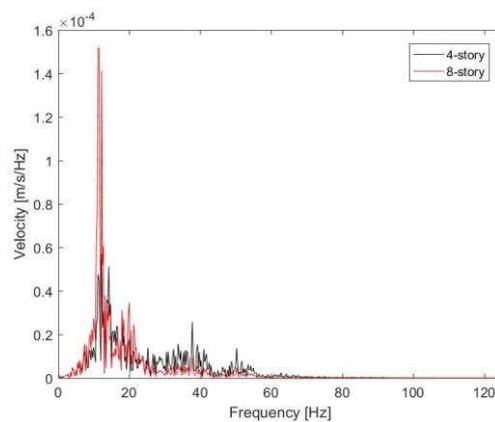


*Figure 25 – Frequency content comparison*
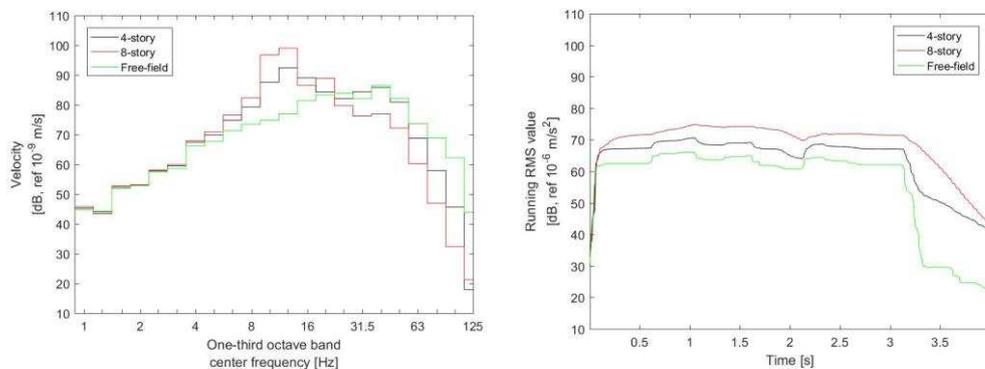


*Figure 26 – Building/soil response to vibration (Left: 1/3 Octave comparison, Right: running RMS)*

## 5.  Conclusion

Ground-borne vibration from railway defects is a growing problem, particularly in urban areas.  Therefore this work proposes a hybrid time-frequency methodology to simulate the generation of vibration at rail defects and its propagation through the track, soil and into nearby buildings.  To do so, the force density due to wheel-rail interaction at the defect location is calculated using a finite element track-soil model, coupled with a multi-body dynamic vehicle model.  The transfer function between track and soil is calculated using a 2.5D finite element approach and then coupled with the force densities to obtain the free-field response.  Finally, an approach formulated in the time domain

is used to compute the soil-structure interaction and the response of buildings close to the line. The effect of defect type, train speed and building type (4 vs 8 storey) is analysed. It is found that train speed doesn't correlate with building vibration and that different defect types have a complex relationship with vibration levels both in the ground and buildings. The 8 storey building has a frequency response dominated by a narrow frequency range, whereas the mode shapes of the 4 storey building are spread over a broader frequency band. This results in the 8 storey building have a higher response for all vibration metrics considered.

## Acknowledgements

## References

1       Connolly DP, Marecki GP, Kouroussis G, Thalassinakis I, Woodward PK. The growth of railway ground vibration problems - A review. *Sci Total Environ* 2015; **568**:1276–1282.

2       Mouzakis C, Vogiatzis K, Zafiropoulou V. Assessing subway network ground borne noise and vibration using transfer function from tunnel wall to soil surface measured by muck train operation. *Sci Total Environ* 2019; **650**:2888–2896.

3       Vogiatzis K, Mouzakis H. Ground-borne noise and vibration transmitted from subway networks to multi-storey reinforced concrete buildings. *Transport* 2017; **33**:1–8.

4       Zhu S, Yang J, Yan H, Zhang L, Cai C. Low-frequency vibration control of floating slab tracks using dynamic vibration absorbers. *Veh Syst Dyn* 2015; **53**:1296–1314.

5       Zhu S, Wang J, Cai C, Wang K, Zhai W, Yang J, *et al.* Development of a Vibration Attenuation Track at Low Frequencies for Urban Rail Transit. *Comput Civ Infrastruct Eng* 2017; **32**:713–726.

6       Iwnicki S. *Handbook of Railway Vehicle Dynamics*. ; 2006.

7       Lombaert G, Degrande G. Ground-borne vibration due to static and dynamic axle loads of InterCity and high-speed trains. *J Sound Vib* 2009; **319**:1036–1066.

8       Vermeulen PJ, Johnson KL. Contact of nonspherical elastic bodies transmitting tangential forces. *Trans ASME* 1964.

9       Carter FW. On the action of a locomotive driving wheel. *Proc R Soc London* 1926; **112**:151–157.

10      Kalker J. A strip theory for rolling with slip and spin. *Proc Kon Ned Akad van Wetenachappen* 1966; **B70**:10–62.

11      Pombo J, Ambrósio J, Silva M. A new wheel-rail contact model for railway dynamics. *Veh Syst Dyn* 2007; **45**:165–189.

12      Carlberger A, Torstensson PT, Nielsen JCO, Frid A. An iterative methodology for the prediction of dynamic vehicle–track interaction and long-term periodic rail wear. *Proc Inst Mech Eng Part F J Rail Rapid Transit* 2018; **232**:1718–1730.

13    Antunes P, Magalhães H, Ambrósio J, Pombo J, Costa J. A co-simulation approach to the wheel–rail contact with flexible railway track. *Multibody Syst Dyn* Published Online First: 2018. doi:10.1007/s11044-018-09646-0

14    Nielsen JCO, Abrahamsson TJS. Coupling of physical and modal components for analysis of moving non-linear dynamic systems on general beam structures. *Int J Numer Methods Eng* 1992; **33**:1843–1859.

15    Zhai W, Sun X. A Detailed Model for Investigating Vertical Interaction between Railway Vehicle and Track. *Veh Syst Dyn* 1994; **23**:603–615.

16    Oscarsson J, Dahlberg T. Dynamic Train/Track/Ballast Interaction - Computer Models and Full-Scale Experiments. *Veh Syst Dyn* 1998; **29**:73–84.

17    Younesian D, Marjani SR, Esmailzadeh E. Importance of flexural mode shapes in dynamic analysis of high-speed trains traveling on bridges. *JVC/Journal Vib Control* 2014; **20**:1565–1583.

18    Zhao X, Li Z, Liu J. Wheel-rail impact and the dynamic forces at discrete supports of rails in the presence of singular rail surface defects. *Proc Inst Mech Eng Part F J Rail Rapid Transit* 2012; **226**:124–139.

19    Grossoni I, Iwnicki S, Bezin Y, Gong C. Dynamics of a vehicle–track coupling system at a rail joint. *J rail rapid transit* 2015; **229**:364–374.

20    Alexandrou G, Kouroussis G, Verlinden O. A comprehensive prediction model for vehicle/track/soil dynamic response due to wheel flats. *Proc Inst Mech Eng Part F J Rail Rapid Transit* 2015; **230**:1088–1104.

21    Kouroussis G, Connolly DP, Alexandrou G, Vogiatzis K. The effect of railway local irregularities on ground vibration. *Transp Res Part D Transp Environ* 2015; **39**:17–30.

22    Kouroussis G, Connolly DP, Alexandrou G, Vogiatzis K. Railway ground vibrations induced by wheel and rail singular defects. *Veh Syst Dyn* Published Online First: 2015. doi:10.1080/00423114.2015.1062116

23    Kouroussis G, Vogiatzis KE, Connolly DP. A combined numerical/experimental prediction method for urban railway vibration. *Soil Dyn Earthq Eng* 2017; **97**:377–386.

24    Federal Railroad Administration. High-Speed Ground Transportation Noise and Vibration Impact Assessment. U.S. Department of Transportation. ; 2012.

25    Rossi F, Nicolini A. A simple model to predict train-induced vibration: theoretical formulation and experimental validation. *Environ Impact Assess Rev* 2003; **23**:305–322.

26    With C, Bahrekazemi M, Bodare A. Validation of an empirical model for prediction of train-induced ground vibrations. *Soil Dyn Earthq Eng* 2006; **26**:983–990.

27    Hussein MFM, Hunt HEM, Rikse L, Gupta S, Degrande G. Using the PiP Model for Fast Calculation of Vibration from a Railway Tunnel in a Multi-layered Half-Space. ; :136–142.

28    Verbraken H, Lombaert G, Degrande G. Experimental and numerical prediction of railway induced vibration. 2012; **13**:802–813.

29    Triepaischajonsak N, Thompson DJ, Jones CJC, Ryue J, Priest J a. Ground vibration from trains: experimental parameter characterization and validation of a numerical model. *Proc Inst Mech Eng Part F J Rail Rapid Transit* 2011; **225**:140–153.

30    Connolly DP, Kouroussis G, Woodward PK, Giannopoulos A, Verlinden O, Forde MC. Scoping prediction of re-radiated ground-borne noise and vibration near high speed rail lines with variable soils. *Soil Dyn Earthq Eng* 2014; **66**:78–88.

31    Connolly DP, Kouroussis G, Giannopoulos A, Verlinden O, Woodward PK, Forde MC. Assessment of railway vibrations using an efficient scoping model. *Soil Dyn Earthq Eng* 2014; **58**:37–47.

32    Galvín P, Mendoza DL, Connolly DP, Degrande G, Lombaert G, Romero A. Scoping assessment of free-field vibrations due to railway traffic. *Soil Dyn Earthq Eng* 2018; **114**:598–614.

33    François S, Galvín P, Schevenels M, Lombaert G, Degrande G. A 2.5D coupled FE-BE methodology for the prediction of railway induced vibrations. *Notes Numer Fluid Mech Multidiscip Des* 2012; **118**:367–374.

34    Alves Costa P, Calçada R, Silva Cardoso  a. Track–ground vibrations induced by railway traffic: In-situ measurements and validation of a 2.5D FEM-BEM model. *Soil Dyn Earthq Eng* 2012; **32**:111–128.

35    Yang Y Bin, Hung HH. A 2.5D finite/infinite element approach for modelling visco-elastic bodies subjected to moving loads. *Int J Numer Methods Eng* 2001; **51**:1317–1336.

36    Hung HH, Chen GH, Yang YB. Effect of railway roughness on soil vibrations due to moving trains by 2.5D finite/infinite element approach. *Eng Struct* 2013; **57**:254–266.

37    Yang YB, Hung HH. Soil Vibrations Caused by Underground Moving Trains. *J Geotech Geoenvironmental Eng* 2008; **134**:1633–1644.

38    Kouroussis G, Verlinden O, Conti C. Prediction of Ground Vibrations Induced By Railway Traffic: an Analysis of the Modelling Assumptions of Vehicle, Track Soil and Buildings. 2013; **18**:163–172.

39    Francois S, Pyl L, Masoumi H, Degrande G. The influence of dynamic soil–structure interaction on traffic induced vibrations in buildings. *Soil Dyn Earthq Eng* 2007; **27**:655–674.

40    Hussein M, Hunt H, Kuo K, Alves Costa P, Barbosa J. The use of sub-modelling technique to calculate vibration in buildings from underground railways. *Proc Inst Mech Eng Part F J Rail Rapid Transit* Published Online First: 27 November 2013. doi:10.1177/0954409713511449

41    Auersch L. Building Response due to Ground Vibration — Simple Prediction Model Based on Experience with Detailed Models and Measurements. *Int J Acoust Vib* 2010; **15**:101–112.

42    López-Mendoza D, Romero A, Connolly DP, Galvín P. Scoping assessment of building vibration induced by railway traffic. *Soil Dyn Earthq Eng* 2017; **93**:147–161.

43    Kouroussis G, Florentin J, Verlinden O. Ground vibrations induced by InterCity/InterRegion trains: A numerical prediction based on the multibody/finite element modeling approach. *JVC/Journal Vib Control* 2016; **22**:4192–4210.

44    Kouroussis G, Connolly DP, Verlinden O. Railway induced ground vibrations - a review of vehicle effects. *Int J Rail Transp* 2014; **2**:69–110.

45    Mezher SB, Connolly DP, Woodward PK, Laghrouche O, Pombo J, Costa PA. Railway critical velocity - Analytical prediction and analysis. *Transp Geotech* Published Online First: 2015. doi:10.1016/j.trgeo.2015.09.002

46    Auersch L, Romero A, Galvin P. Building dynamic response due to incident wave field considering soil-structure interaction. *Rev Int Métodos Numéricos para Cálculo y Diseño en*

*Ing* 2014; **30**:256–263.

47      Auersch L. Dynamic Stiffness of Foundations on Inhomogeneous Soils for a Realistic Prediction of Vertical Building Resonance. *J Geotech Geoenviromental Eng* 2008; **134**:328–341.

48      Auersch L. Wave propagation in the elastic half-space due to an interior load and its application to ground vibration problems and buildings on pile foundations. *Soil Dyn Earthq Eng* 2010; **30**:925–936.

49      Fiala P, Degrande G, Augusztinovicz F. Numerical modelling of ground-borne noise and vibration in buildings due to surface rail traffic. *J Sound Vib* 2007; **301**:718–738.

50      U.S. Department of Commerce. Soil-Structure Interaction for Building Structures (Report: NIST GCR 12-917-21). ; 2012. doi:12-917-21

51      Schwingungsmessung an Schienenverkehrswegen - Teil 1: Messverfahren für Schwingungen (DIN 45672-1:2018-02).

52      BSI Standards Publication Mechanical vibration and shock — Evaluation of human exposure to whole-body vibration Part 1 : General Requirements. 1997.

53      Deutsches Institut fur Normung. DIN 4150-3: Structural vibrations - Part 3: Effects of vibration on structures. ; 1999.

54      Kouroussis G, Connolly DP, Vogiatzis K, Verlinden O. Modelling the environmental effects of railway vibrations from different types of rolling stock - A numerical study. *Shock Vib* Published Online First: 2015. doi:10.1155/2015/142807

55      Hiller M. Dynamics of Multibody Systems with Minimal Coordinates. In: *Computer-Aided Analysis of Rigid and Flexible Mechanical Systems, Proceedings of the NATO Advanced Study Institute*.; 1993. pp. 119–163.

56      Olivier B, Connolly DP, Alves Costa P, Kouroussis G. The effect of embankment on high speed rail ground vibrations. *Int J Rail Transp* 2016; **4**:229–246.

57      Kouroussis G, Connolly DP, Olivier B, Laghrouche O, Alves Costa P. Railway cuttings and embankments: Experimental and numerical studies of ground vibration. *Sci Total Environ* 2016; **557**–**558**:110–122.

58      Kouroussis G, Gazetas G, Anastasopoulos I, Conti C, Verlinden O. Discrete modelling of vertical track–soil coupling for vehicle–track dynamics. *Soil Dyn Earthq Eng* 2011; **31**:1711–1723.

59      Galvín P, Romero A. A MATLAB toolbox for soil-structure interaction analysis with finite and boundary elements. *Soil Dyn Earthq Eng* 2014; **57**:10–14.

60      Kouroussis G, Olivier B, Romero A, Galvin P, Connolly DP. A fast numerical assessment of railway-induced ground vibration in urban conditions. In: *Proceedings of the 25th International Congress on Sound and Vibration*.; 2018.

61      Madshus C, Kaynia AM. High-Speed Railway Lines on Soft Ground: Dynamic Behaviour At Critical Train Speed. *J Sound Vib* 2000; **231**:689–701.

62      Dong K, Connolly DP, Laghrouche O, Woodward PK, Costa PA. The stiffening of soft soils on railway lines. *Transp Geotech* Published Online First: 2018. doi:https://doi.org/10.1016/j.trgeo.2018.09.004

63      Connolly DP, Kouroussis G, Woodward PK, Costa PA, Verlinden O, Forde MC. Field testing and analysis of high speed rail vibrations. *Soil Dyn Earthq Eng* Published Online First: 2014. doi:10.1016/j.soildyn.2014.08.013

64      Degrande G, Schillemans L. Free Field Vibrations During the Passage of a Thalys High-Speed Train At Variable Speed. *J Sound Vib* 2001; **247**:131–144.